Nano Res. 2012, 5(8): 543–549
DOI 10.1007/s12274-012-0239-9
Research Article

ISSN 1998-0124
CN 11-5974/O4

Sequential Assembly of Metal-Free Phthalocyanine on Few-Layer Epitaxial Graphene Mediated by Thickness-Dependent Surface Potential

Yabo Gao[1], Yanfeng Zhang[1] (✉), Jun Ren[2], Denghua Li[3], Teng Gao[1], Ruiqi Zhao[1], Yanlian Yang[3], Sheng Meng[2], Chen Wang[3], and Zhongfan Liu[1] (✉)

[1] Center for Nanochemistry (CNC), Beijing National Laboratory for Molecular Sciences, State Key Laboratory for Structural Chemistry of Unstable and Stable Species, College of Chemistry and Molecular Engineering, Academy for Advanced Interdisciplinary Studies, Peking University, Beijing 100871, China
[2] Beijing National Laboratory for Condensed Matter Physics, Institute of Physics, Chinese Academy of Sciences, Beijing 100190, China
[3] National Center for Nanoscience and Technology, Beijing 100190, China

Received: 22 December 2011 / Revised: 18 February 2012 / Accepted: 7 June 2012

ABSTRACT

Due to strong interactions between epitaxial graphene and SiC(0001) substrates, the overlayer charge density induced by the interface charging effect is much more attenuated than that of exfoliated graphene on SiO_2. We report herein a quantitive detection of the charge properties of few-layer graphene by surface potential measurements using electrostatic force microscopy (EFM). A minor difference in surface potential is observed to mediate a sequential assembly of metal-free phthalocyanine (H_2Pc) on monolayer, bilayer and trilayer graphenes, as demonstrated by scanning tunneling microscopy (STM). In order to understand this, we further executed density functional theory (DFT) calculations which showed higher adsorption energies for Pc on thinner graphenes. In this case, we attribute the unique growth behavior of Pc to its variable adsorption energies on few-layer graphene, and in turn the layer charge variations from the viewpoint of energy minimizations. This work is expected to provide fundamental data useful for related nanodevice fabrications.

KEYWORDS

Scanning tunneling microscopy (STM), epitaxial graphene, phthalocyanine, self-assembly, electrostatic force microscopy (EFM)

1. Introduction

Few-layer graphenes with their thickness varying from monolayer to multilayers offer an intriguing template, on which the native surface properties such as surface potential, work function, and the surface processes such as oxygen etching kinetics, hydrogenation capability and nucleation of metal atoms can be tuned in terms of the number of graphene atomic layers [1–6]. In particular, deliberate p- or n-doping and chemical modification of graphene by decorating functional molecules have attracted wide attention by virtue of their capabilities of tuning the transport properties such as the carrier mobility of graphene [7–14]. However, the adsorption configurations of molecules, the existing interactions between molecule and substrate, and

Address correspondence to Yanfeng Zhang, yanfengzhang@pku.edu.cn; Zhongfan Liu, zfliu@pku.edu.cn

more importantly, why the properties can be tuned by the thickness of graphene are still unclear at an atomic-scale level. Scanning tunneling microscope/spectroscopy (STM/STS) can serve as an effective analytical method for obtaining these details [15, 16].

Graphene epitaxially (EG) grown on SiC(0001) is weakly n-doped by depletion of electrons from n-type SiC [17]. The electrostatic interactions within few-layer graphene and SiC(0001) substrates are deemed to imply effects on the surface potentials of few-layer graphene, and their variations with thickness can be utilized to quantify layer charge distributions. Some published experiments have dealt with this interface electrostatic interaction between exfoliated graphene on SiO_2, and between graphene and SiC(0001) [18, 19].

In this work, we accomplished the native charge transfer measurement on few-layer EG on SiC(0001) through surface potential measurements using electrostatic force microscopy (EFM). The surface potentials from monolayer to trilayer graphene show a minor difference, falling in the range of 20 meV. In order to visualize this, metal-free phthalocyanine (H_2Pc or simply Pc) was then selected as a molecule tracer, and its assembly on few-layer graphene is expected to be directed by the different substrate electronic properties. In a further step, DFT calculations were executed to obtain the diffusion barrier, as well as the adsorption energy of Pc as a function of graphene thickness in order to make a reliable illustration of the experimental data. The consistent theoretical and experimental results suggest that the sequential assembly of Pc on few-layer coexisting graphene is probably mediated by the thickness-dependent local surface potential of epitaxial graphene.

2. Experimental

An n-doped 6H-SiC(0001) with carrier density of 10^{16} cm^{-3} was used as the substrate, and was first degassed at 850 ℃ and then heated to 1400 ℃ for graphene growth inside an ultrahigh vacuum (UHV) system. Pc (Alfa-Aesar company) molecules were deposited by heating a tantalum container to ~270 ℃, in equivalence to an approximate evaporation rate of 0.3 Å/min. STM experiments were carried out in another chamber of the UHV system. EFM measurements were performed on a Veeco Dimension Icon Atomic Force Microscopy (AFM) system. A conductive tip was used for recording sample topography and EFM phase in a two-pass mode.

First-principles calculations were performed within the framework of density functional theory (DFT) as implemented in SIESTA [20]. We used pseudopotentials of the Troullier–Martins type, the local-density approximation (LDA) and van der Waals density functional (vdW-DF) for exchange-correlation energy, and a local basis set of double polarized orbitals (13 orbitals for C, N, O and 5 for H) [16]. An auxiliary real-space grid equivalent to a plane-wave cutoff of 120 Ry and *k*-point mesh of (8 × 8 × 1) in Monkhorst–Pack sampling was employed. Basis-set superposition errors were excluded in relative energies. The atomic structure was considered fully relaxed when the magnitude of forces on every atom was smaller than 0.04 eV/Å.

3. Results and discussion

The preparation of EG on SiC(0001) substrates and the surface characteristics have been well investigated by STM (not shown here [21–26]). On account of the unique growth process, via decomposition of SiC and desorption of Si, different layered graphenes usually coexist on SiC(0001). It is known that the reconstructed carbon-rich interface layer possesses a native surface corrugation, which can propagate into upper graphene layers and result in decayed surface undulations. By virtue of this fact, the film thickness is correlated strictly with the surface roughness, as can be quantificationally identified from STM line-profile analyses. This is clearly seen in Figs. 1(a)–1(d) showing 0L (or carbon-rich interface layer), 1L, 2L EG. As shown in the table in Fig. 1(e), a one-to-one correspondence between layer thickness and surface roughness was established according many experimental data, hence providing a reliable background for layer thickness determination.

As has been recently demonstrated by angle-resolved photoemission spectroscopy data (ARPES), the EG/SiC(0001) system is very special by virtue of its weakly n-doped feature, and the charge density varies with graphene thickness [17]. It is rational to expect that this substrate effect will have a negligible influence on surface potentials (or surface electron

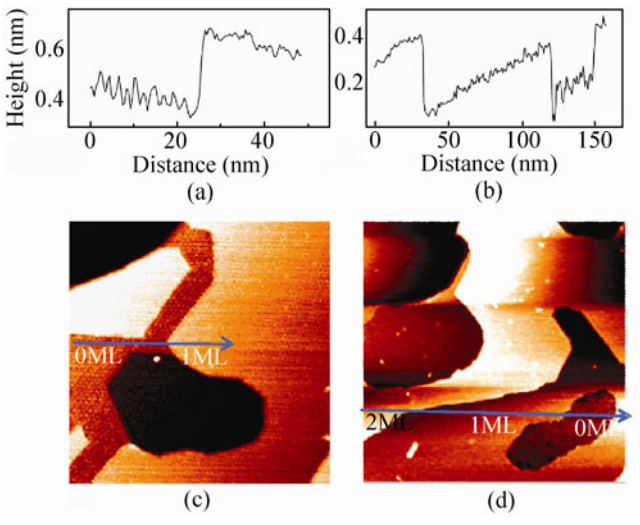

Graphene thickness	Surface roughness	Tunneling condition
0L	0.10 nm ± 0.03 nm	0.01 V, 2 nA
1L	0.06 nm ± 0.03 nm	0.01 V, 2 nA
2L	0.04 nm ± 0.03 nm	0.01 V, 2 nA
3L	0.02 nm ± 0.05 nm	0.01 V, 2 nA

(e)

Figure 1 Section-views ((a), (b)), corresponding STM morphologies ((c), (d)), and statistical data (e) showing interface reconstruction-induced graphene surface roughness alternations with the method used in Ref. [22]

densities) of few-layer graphene which is measureable by EFM. A recent result demonstrates this thickness-dependent local electrical property, but showing only small differences between few-layer graphene samples [19]. In order to visualize this effect, phthalocyanine (Pc), as a conjugated π-electron system and an electron acceptor, was used as a molecule tracer. Differently charged graphene layers are expected to mediate the surface assembly process of Pc, as schematically shown in Fig. 2.

The local surface potential measurement was performed using the same method as reported in recent work [18, 19, 27]. The topography and EFM phase images were obtained in a two-pass lift mode, in which the EFM images follow the topographic profile at a fixed lift height (h) above the sample surface. A conductive AFM tip is biased with a DC voltage (V_{tip}) and the substrate is grounded. By modeling the cantilever as a harmonic oscillator, the phase shift $\Delta\Phi$ between the cantilever oscillation and the driving

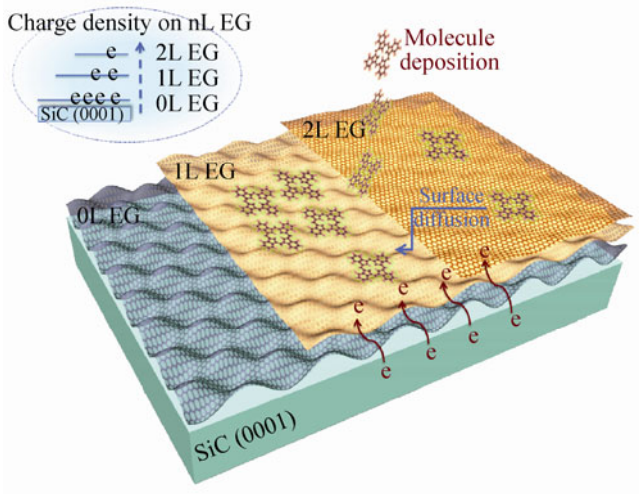

Figure 2 Displayed in the upper left panel is a schematic drawing of the charge densities on few-layer EG. The deposition and surface diffusion of Pc molecules, as well as the assembly of Pc into molecule domains are all schematically shown

force equals $\Delta\varphi - \pi/2$, where $\Delta\varphi$ over the sample due to tip-sample capacitive coupling, the spring constant k, and quality factor Q can be expressed as

$$\Delta\Phi = -\frac{Q}{2k}C''(h)(V_{tip} - V_s)^2 \quad (1)$$

where $C''(h)$ is the second derivative of the tip-sample capacitance as a function of h, and V_s is the local electrostatic potential on the sample surface [18, 28, 29]. Obviously, the phase shift is zero when V_{tip} equals V_s.

Shown in Fig. 3 is the AFM morphology (Fig. 3(a)) and EFM phase images at opposite biases (Figs. 3(b) and 3(c)). It is clear to see that the contour of the phase image in Fig. 3(b) agrees well with the AFM topography in Fig. 3(a), where a bilayer graphene has a higher contrast in the AFM morphology and EFM phase image than that of monolayer. The different contrasts in Fig. 3(b) illustrate dissimilar surface potentials for various graphene layers, as deduced from Eq. (1). When the tip bias turns into negative polarity with $V_{tip} = -2$ V, the contrast of the EFM phase image is inverted accordingly (Fig. 3(c)). This confirms the reliability of the EFM measurements. In order to obtain the surface potential image of few-layer graphene, both an alternating current (AC) voltage at the resonance frequency of the cantilever and a direct current (DC) voltage were applied to the cantilever. The nulling DC potential to minimize the cantilever

vibration gives rise to the value of surface potential. As a result, the local surface potential shown in Fig. 3(d) demonstrates a monotonic increase with the increase of graphene thickness. The corresponding high-resolution images in Figs. 3(e)–3(h) support this conclusion. According to the section-view of Fig. 3(h), the measured surface potential difference between monolayer and bilayer graphene is ~21 mV (Fig. 3(j)).

This disparity in surface potential can be reconfirmed by plotting the EFM phase shift ($\Delta\Phi$) as a function of V_{tip} (Fig. 3(i)). According to Eq. (1), the apex of the parabolic fitting of the plot corresponds to V_s, and the shift of V_s can be deduced to be ~23 mV. This value corresponds well with the above straightforward surface potential measurement (~21 mV).

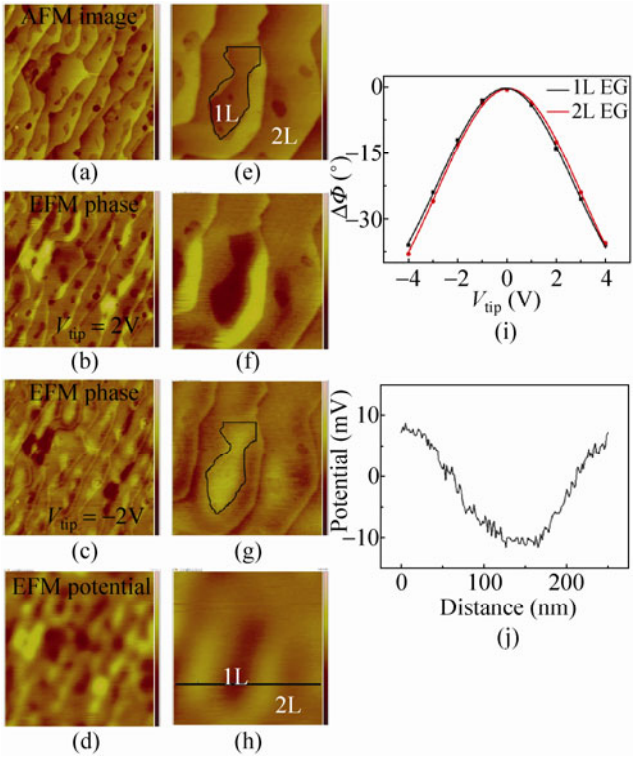

Figure 3 (a) (2000 nm × 2000 nm) AFM image of few-layer graphene on SiC(0001) with the thicknesses range from 0L to 3L. The *z*-scale of the color bar is 0–4 nm. (b), (c) Corresponding EFM phase shift images with V_{tip} = 2 V and V_{tip} = –2 V, respectively. The *z*-scale of the color bar is 0–50°. (d) Surface potential image by applying a drive amplitude V_{drive} = 5 V. The *z*-scale of the color bar is 0–100 meV. (e)–(h) (600 nm × 600 nm) High-resolution images corresponding to (a)–(d). (i) EFM phase shift ($\Delta\Phi$) plotted as a function of V_{tip} for 1L (in black) and 2L (in red) graphene. (j) Sectional profile along the line in (h). The *z*-scale of the color bar in (e)–(h) is the same as in (a)–(d)

However, it is only one tenth that of exfoliated graphene on SiO_2. The remarkable attenuation can be explained by the strong coupling of epitaxial graphene with the underlying SiC(0001) substrate [18].

H_2Pc, as a π-conjugated system (shown in Fig. 4(a)), was then deposited on few-layer coexisting substrates kept at room temperature. In ordering to obtain stable STM images, the as-grown sample was usually annealed at room temperature for several hours prior to observations [30–32]. Figures 4(b) and 4(c) present large-scale STM images at Pc coverage of 0.3 monolayer (ML) and 0.5 ML, respectively. Note that Pc adsorption on monolayer graphene (circled by dashed lines) can be easily recognized by its remarkably lower STM contrast than that of neighboring bare graphene (Fig. 4(b)). Interestingly, Pc adlayers occupy only part of the 1L EG while the rest areas of 2L and 3L are free of the molecule. Together with the increase of Pc deposition, molecule domains start to evolve on bilayer graphene, as exemplified in Fig. 4(c). In molecule scales, the hexagonal molecule lattice in the insert of Fig. 4(c), showing absolute values of the base vectors $|a|$=

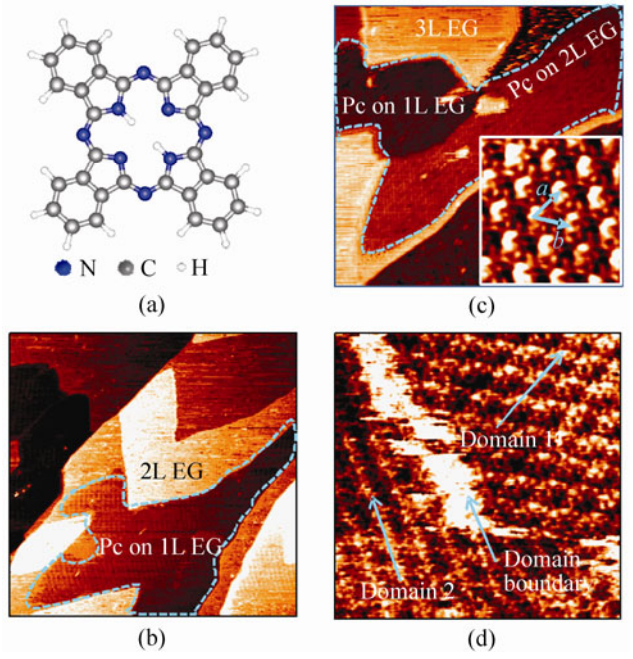

Figure 4 (a) Molecule structure of H_2Pc. (b) (425 nm × 425 nm, V_{bias} = –0.02 V, I_t = 1.40 nA) STM morphology of 0.3 ML Pc deposition on few-layer coexisting graphene. (c) (170 nm × 170 nm; V_{bias} = –0.77 V, I_t = 0.54 nA) Assembly of 0.5 ML Pc. (d) (11 nm × 11 nm; V_{bias} = –0.21 V, I_t = 0.66 nA) Close-up views on 1L EG showing two Pc domains

$|b|$=1.75 nm ± 0.05 nm, again illustrate a perfect two-dimensional assembly of Pc. Inside a graphene terrace, two Pc domains with their orientations rotated by 60° can be easily seen in Fig. 4(d). More systematic STM examinations reveal that the orientations of Pc domains are usually differentiated by a multiple of 60°. This preferred orientation accounts for the limited diffusion length of adsorbed Pc molecules over graphene terraces generally having dimensions of ~30 nm × 30 nm.

A question arises as to what is the major mechanism for this preferred occupation of Pc on thinner graphene than that of thicker ones? It should be kinetic or thermodynamic, and influenced by a number of parameters such as sample temperature, surface topography and electronic density of states (DOS) [33, 34]. Given the limited timescale resolution of STM, the dynamic process cannot be effectively imaged at this moment.

First-principles calculations based on DFT were then performed to answer this question [35]. The slightly smaller supercell of (4, 3) × (3, 4) (here (n, m) denotes the vector which is the sum of n and m multiples of two primitive vectors of graphene) was chosen for calculating the interaction between Pc molecules and graphene substrate which is dominant and prevails over intermolecular interaction [16]. The molecule was modeled to be staying on the graphene surface with a flat lying geometry, as exemplified in Fig. 5(a). The adsorption height of H_2Pc on graphene was calculated to be 3.17 Å (LDA) and 3.47 Å (vdW-DF), respectively.

The energetic factor could be the major reason, i.e. due to the lower chemical potential in one region compared with that in another, and the accumulation of adatoms or molecules in this region can lead to a lower system total energy. To confirm this, Pc adsorption on few-layer graphene was modeled by assuming graphene with different local charges. The adsorption energies were calculated to be 2.49 eV, 2.66 eV, 2.83 eV for graphene charged with 0.0025 e, 0.005 e, 0.0075 e per carbon atom, or roughly corresponding to 3, 2, 1 graphene layers, as exemplified in the plot of Fig. 5(c). The adsorption energies with respect to the carbon lattice, defined as the projection of the geometry center of the H_2Pc molecule onto the carbon lattice of graphene, are 2.41 eV on top sites,

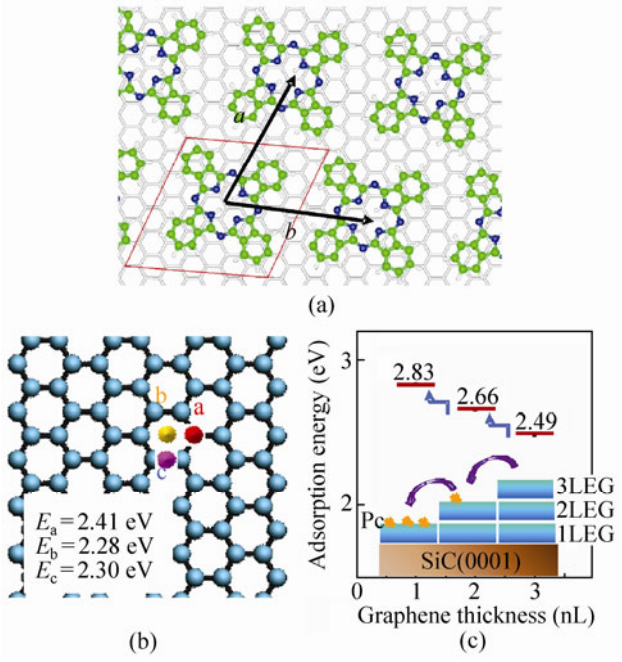

Figure 5 (a) Simulated data of Pc assembly on epitaxial graphene. (b) First-principles DFT calculations of adsorption energies of Pc on a top site (a, 2.41 eV), hollow site (b, 2.28 eV) and bridge site (c, 2.30 eV) of the carbon lattice. (c) Adsorption energies of Pc calculated as a function of graphene thickness

2.28 eV on hollow sites and 2.30 eV on bridge sites (Fig. 5(b)). This indicates an easy diffusion of Pc over the graphene surface with an energy barrier of 2.41 – 2.30 ≈ 0.11 eV, which is much smaller than the adsorption of Pc on graphene. Hence, the kinetically limited process may not be crucial.

The energy difference between monolayer and bilayer graphene was 0.17 eV. This energy difference is proposed to drive the preferential adsorption/assembly of Pc on monolayer graphene from the viewpoint of total energy minimization. For the same reason, preferred Pc adsorptions on bilayer graphene can be understandable at an even higher Pc coverage.

4. Conclusions

We have revealed the different surface potentials or surface charge densities of few-layer epitaxial graphene on SiC(0001) using EFM. Although a minor difference (of ~20 meV) between monolayer and bilayer graphene is obtained, the values are much lower than that of exfoliated graphenes on SiO_2, and the Pc assembly related to molecule–substrate interactions through

donor–acceptor interactions is proposed to be tuned in terms of one graphene layer at a time. Accordingly, Pc molecules preferentially diffuse to monolayer, bilayer, and trilayer regions to form compact 2D domains, showing a clear thickness-dependent effect. This experimental result is confirmed by calculating the adsorption energy of Pc on graphene using DFT calculations, where Pc adsorption on thinner graphenes has higher adsorption energies. Therefore, the sequential assembly behavior is understandable from the viewpoint of energy minimization. In essence, this preferred assembly behavior is mediated by the differently charged few-layer graphene materials arising from interlayer charging effects.

As the adsorbed molecules can exert additional influence on the electronic properties such as the carrier mobility of graphene, this work provides not only an intriguing example of thickness-dependent surface assembly but offers valuable information about controllable nanodevice fabrications.

Acknowledgements

This work was financially supported by the National Natural Science Foundation of China (Grants Nos. 21073003, 20973013, 51072004, 50821061, and 20833001), the Ministry of Science and Technology of China (Grants Nos. 2011CB921903, 2012CB921404, 2007CB936203, and 2007CB936802) and the Foundation for the Authors of National Excellent Doctoral Dissertations of China (No. 201087).

References

[1] Filleter, T.; Emtsev, K. V.; Seyller, Th.; Bennewitz, R. Local work function measurements of epitaxial graphene. *Appl. Phys. Lett.* **2008**, *93*, 133117.

[2] Lee, N. J.; Yoo, J. W.; Choi, Y. J.; Kang, C. J.; Jeon, D. Y.; Kim, D. C.; Seo, S.; Chung, H. J. The interlayer screening effect of graphene sheets investigated by Kelvin probe force microscopy. *Appl. Phys. Lett.* **2009**, *94*, 222107.

[3] Liu, L.; Ryu, S. M.; Tomasik, M. R.; Stolyarova, E.; Jung, N.; Hybertsen, M. S.; Steigerwald, M. L.; Brus, L. E.; Flynn, G. W. Graphene oxidation: Thickness-dependent etching and strong chemical doping. *Nano Lett.* **2008**, *8*, 1965–1970.

[4] Luo, Z. Q.; Yu, T.; Kim, K.; Ni, Z. H.; You, Y. M.; Lim, S. H.; Shen, Z. X.; Wang, S. Z.; Lin, J. Y. Thickness-dependent reversible hydrogenation of graphene layers. *ACS Nano* **2009**, *3*, 1781–1788.

[5] Luo, Z. T.; Somers, L. A.; Dan, Y. P.; Ly, T.; Kybert, N. J.; Mele, E. J.; Johnson, A. T. C. Size-selective nanoparticle growth on few-layer graphene films. *Nano Lett.* **2010**, *10*, 777–781.

[6] Zhou, H. Q.; Qiu, C. Y.; Liu, Z.; Yang, H. C.; Hu, L. J.; Liu, J.; Yang, H. F.; Gu, C. Z.; Sun, L. F. Thickness-dependent morphologies of gold on n-layer graphenes. *J. Am. Chem. Soc.* **2010**, *132*, 944–946.

[7] Ohta, T.; Bostwick, A.; Seyller, Th.; Horn, K.; Rotenberg, E. Controlling the electronic structure of bilayer graphene. *Science* **2006**, *313*, 951–954.

[8] Chen, W.; Chen, S.; Qi, D. C.; Gao, X. Y.; Wee, A. T. S. Surface transfer p-type doping of epitaxial graphene. *J. Am. Chem. Soc.* **2007**, *129*, 10418–10422.

[9] Wehling, T. O.; Novoselov, K. S.; Morozov, S. V.; Vdovin, E. E.; Katsnelson, M. I.; Geim, A. K.; Lichtenstein, A. I. Molecular doping of graphene. *Nano Lett.* **2008**, *8*, 173–177.

[10] Lu, Y. H.; Chen, W.; Feng, Y. P.; He, P. M. Tuning the electronic structure of graphene by an organic molecule. *J. Phys. Chem. B* **2009**, *113*, 2–5.

[11] Coletti, C.; Riedl, C.; Lee, D. S.; Krauss, B.; Patthey, L.; von Klitzing, K.; Smet, J. H.; Starke, U. Charge neutrality and band-gap tuning of epitaxial graphene on SiC by molecular doping. *Phys. Rev. B* **2010**, *81*, 235401.

[12] Wang, X. M.; Xu, J. B.; Xie, W. G.; Du, J. Quantitative analysis of graphene doping by organic molecular charge transfer. *J. Phys. Chem. C* **2011**, *115*, 7596–7602.

[13] Koehler, F. M.; Jacobsen, A.; Ensslin, K.; Stampfer, C.; Stark, W. J. Selective chemical modification of graphene surfaces: Distinction between single and bilayer graphene. *Small* **2010**, *6*, 1125–1130.

[14] Koehler, F. M.; Luechinger, N. A.; Ziegler, D.; Athanassiou, E. K.; Grass, R. N.; Rossi, A.; Hierold, C.; Stemmer, A.; Stark, W. J. Permanent pattern-resolved adjustment of the surface potential of graphene-like carbon through chemical functionalization. *Angew. Chem. Int. Ed.* **2009**, *48*, 224–227.

[15] Zhao, R. Q.; Zhang, Y. F.; Gao, T.; Gao. Y. B.; Liu, N.; Fu, L.; Liu, Z. F. Scanning tunneling microscope observations of non-AB stacking of graphene on Ni films. *Nano Res.* **2011**, *4*, 712–721

[16] Wang, Y. L.; Ren, J.; Song, C. L.; Jiang, Y. P.; Wang, L. L.; He, K.; Chen, X.; Jia, J. F.; Meng, S.; Kaxiras, E.; Xue, Q. K.; Ma, X. C. Selective adsorption and electronic interaction of F_{16}CuPc on epitaxial graphene. *Phys. Rev. B* **2010**, *82*, 245420.

[17] Ohta, T.; Bostwick, A.; McChesney, J. L.; Seyller, Th.;

Horn, K.; Rotenberg, E. Interlayer interaction and electronic screening in multilayer graphene investigated with angle-resolved photoemission spectroscopy. *Phys. Rev. Lett.* **2007**, *98*, 206802.

[18] Datta, S. S.; Strachan, D. R.; Mele, E. J.; Johnson, A. T. C. Surface potentials and layer charge distributions in few-layer graphene films. *Nano Lett*. **2009**, *9*, 7–11.

[19] Burnett, T.; Yakimova, R.; Kazakova, O. Mapping of local electrical properties in epitaxial graphene using electrostatic force microscopy. *Nano Lett* **2011**, *11*, 2324–2328.

[20] Soler, J. M.; Artacho, E.; Gale, J. D.; García, A.; Junquera, J.; Ordejón, P.; Sanchez-Portal, D. The SIESTA method for *ab initio* order-N materials simulation. *J. Phys: Condens. Matter*. **2002**, *14*, 2745–2779.

[21] Emtsev, K. V.; Speck, F.; Seyller, Th.; Ley, L. Interaction, growth, and ordering of epitaxial graphene on SiC(0001) surfaces: A comparative photoelectron spectroscopy study. *Phys. Rev. B* **2008**, *77*, 155303.

[22] Seyller, Th.; Bostwick, A.; Emtsev, K. V.; Horn, K.; Ley, L.; McChesney, J. L.; Ohta, T.; Riley, J. D.; Rotenberg, E.; Speck, F. Epitaxial graphene: A new material. *Phys. StatusSolIdi. B-Basic Solid State Phys.* **2008**, *245*, 1436–1446.

[23] Lauffer, P.; Emtsev, K. V.; Graupner, R.; Seyller, Th.; Ley, L.; Reshanov, S. A.; Weber, H. B. Atomic and electronic structure of Few-layer graphene on SiC(0001) studied with scanning tunneling microscopy and spectroscopy. *Phys. Rev. B* **2008**, *77*, 155426.

[24] Brar, V. W.; Zhang, Y. B.; Yayon, Y.; Ohta, T.; McChesney, J. L.; Bostwick, A.; Rotenberg, E.; Horn, K.; Crommie, M. F. Scanning tunneling spectroscopy of inhomogeneous electronic structure in monolayer and bilayer graphene on SiC. *Appl. Phys. Lett.* **2007**, *91*, 122102.

[25] Stolyarova, E.; Rim, K. T.; Ryu, S. M.; Maultzsch, J.; Kim, P.; Brus, L. E.; Heinz, T. F.; Hybertsen, M. S.; Flynn, G. W. High-resolution scanning tunneling microscopy imaging of mesoscopic graphene sheets on an insulating surface. *Proc. Natl. Acad. Sci. USA* **2007**, *104*, 9209–9212.

[26] Riedl, C.; Starke, U.; Bernhardt, J.; Franke, M.; Heinz, K. Structural properties of the graphene-SiC(0001) interface as a key for the preparation of homogeneous large-terrace graphene surfaces. *Phys. Rev. B* **2007**, *76*, 245406.

[27] Curtin, A. E.; Fuhrer, M. S.; Tedesco, J. L.; Myers-Ward, R. L.; Eddy, C. R. Jr.; Gaskill, D. K. Kelvin probe microscopy and electronic transport in graphene on SiC(0001) in the minimum conductivity regime. *Appl. Phys. Lett.* **2011**, *98*, 243111.

[28] Staii, C.; Johnson, A. T.; Pinto, N. J. Quantitative analysis of scanning conductance microscopy. *Nano Lett.* **2004**, *4*, 859–862.

[29] Coffey, D. C.; Ginger, D. S. Time-resolved electrostatic force microscopy of polymer solar cells. *Nat. Mater.* **2006**, *5*, 735–740.

[30] Baffou, G.; Mayne, A. J.; Comtet, G.; Dujardin, G.; Sonnet, Ph.; Stauffer, L. Anchoring phthalocyanine molecules on the 6H-SiC(0001)3×3 surface. *Appl. Phys. Lett.* **2007**, *91*, 073101.

[31] Nilson, K.; Åhlund, J.; Brena, B.; Göthelid, E.; Schiessling, J.; Martensson, N.; Puglia, C. Scanning tunneling microscopy study of metal-free phthalocyanine monolayer structures on graphite. *J. Chem. Phys.* **2007**, *127*, 114702.

[32] Komeda, T.; Isshiki, H.; Liu, J. Metal-free phthalocyanine (H_2Pc) molecule adsorbed on the Au(111) surface: Formation of a wide domain along a single lattice direction. *Sci. Technol. Adv. Mater.* **2010**, *11*, 054602.

[33] Qiu, X. H.; Wang, C.; Zeng, Q. D.; Xu, B.; Yin, S.; Wang, H. N.; Xu, S.; Bai, C. L. Alkane-assisted adsorption and assembly of phthalocyanines and porphyrins. *J. Am. Chem. Soc*. **2000**, *122*, 5550–5556.

[34] Fu, Y. S.; Ji, S. H.; Chen, X.; Ma, X. C.; Wu, R.; Wang, C. C.; Duan, W. H.; Qiu, X. H.; Sun, B.; Zhang, P.; Jia, J. F.; Xue, Q. K. Manipulating the Kondo resonance through quantum size effects. *Phys. Rev. Lett.* **2007**, *99*, 256601.

[35] Ren, J.; Meng, S.; Wang, Y. L.; Ma, X. C.; Xue Q. K. Properties of copper (fluoro-)phthalocyanine layers deposited on epitaxial graphene. *J. Chem. Phys* **2011**, *134*, 194706.